Phase separation in fluids with many interacting components

Krishna Shrinivas[a,1] and Michael P. Brenner[b,c]

[a]NSF–Simons Center for Mathematical & Statistical Analysis of Biology, Harvard University, Cambridge, MA 02138; [b]School of Engineering and Applied Sciences, Harvard University, Cambridge, MA 02138; and [c]Physics Department, Harvard University, Cambridge, MA 02138

Edited by Andrej Kosmrlj, Princeton University, Princeton, NJ, and accepted by the Editorial Board October 3, 2021 (received for review May 6, 2021)

Fluids in natural systems, like the cytoplasm of a cell, often contain thousands of molecular species that are organized into multiple coexisting phases that enable diverse and specific functions. How interactions between numerous molecular species encode for various emergent phases is not well understood. Here, we leverage approaches from random-matrix theory and statistical physics to describe the emergent phase behavior of fluid mixtures with many species whose interactions are drawn randomly from an underlying distribution. Through numerical simulation and stability analyses, we show that these mixtures exhibit staged phase-separation kinetics and are characterized by multiple coexisting phases at steady state with distinct compositions. Random-matrix theory predicts the number of coexisting phases, validated by simulations with diverse component numbers and interaction parameters. Surprisingly, this model predicts an upper bound on the number of phases, derived from dynamical considerations, that is much lower than the limit from the Gibbs phase rule, which is obtained from equilibrium thermodynamic constraints. We design ensembles that encode either linear or nonmonotonic scaling relationships between the number of components and coexisting phases, which we validate through simulation and theory. Finally, inspired by parallels in biological systems, we show that including nonequilibrium turnover of components through chemical reactions can tunably modulate the number of coexisting phases at steady state without changing overall fluid composition. Together, our study provides a model framework that describes the emergent dynamical and steady-state phase behavior of liquid-like mixtures with many interacting constituents.

phase separation | random-matrix theory | multicomponent | multiphase | phase-field simulation

Fluids composed of many components with multiple coexisting phases are widespread in living and soft matter systems. A striking example occurs in the eukaryotic cell, where distinct biochemical pathways are compartmentalized into membraneless organelles called biomolecular condensates, which often form through liquid–liquid phase separation (1–3). Unlike two-phase oil–water mixtures, the cellular milieu is organized into tens of coexisting phases, each of which is enriched in specific biomolecules (1, 2, 4–8). Other prominent examples include microbial ecosystems that organize into fluid-like communities (9–11), self-assembling colloidal systems (12, 13), and synthetic multiphase materials derived from biomolecules (14, 15). Despite their extensive prevalence, our understanding of how microscopic interaction networks between individual constituents encode emergent multiphase behavior remains limited.

Delineating the coexisting phases of a heterogeneous mixture is a problem with a rich history (16)—determined by constraints of chemical, mechanical, and thermal equilibrium. In mixtures with few components (fewer than five), a combination of theory, simulation, and experiment has enabled extensive characterization of phase-separation kinetics and equilibrium coexistence (17–23) and the interplay between phase separation and chemical reactions (19, 24, 25). In the biological context, recent studies have begun to connect biomolecular features to their macroscopic phase behavior in binary or ternary mixtures (7, 26, 27). However, as the number of components increases, determining the emergent phase behavior from the underlying constraints becomes unwieldy and intractable—from both analytical and numerical standpoints, except for very particular systems such as polydisperse blends of a single species (28). An alternate approach, originally proposed by Sear and Cuesta (29), aims to characterize the phase behavior of mixtures that contain many components whose pairwise interactions are drawn from a random distribution. By building on results on properties of random matrices, originally identified by Wigner (30) and subsequently applied in various contexts (31–33), they relate the initial direction of phase separation to properties of the interaction distribution, subsequently confirmed independently by simulation (34). These results, however, are limited to describing only the initial direction of phase separation for marginally stable fluid mixtures (i.e., coinciding exactly at the spinodal). Consequently, little is known about the overall phase behavior of fluid mixtures that spontaneously demix (i.e., within the spinodal)—including kinetics beyond the initial direction of phase separation or the number and composition of coexisting phases at equilibrium. More generally, the emergent phase behavior of fluid mixtures with many randomly interacting components is not well understood. This lack of understanding, in turn, limits our ability to rationally program fluid mixtures with different macroscopic properties.

Significance

Immiscible fluids are found everywhere—examples include vinaigrette and ouzo in the kitchen, multiphase hydrocarbon–water mixtures common in oil extraction, and in virtually all living things. Within the living cell, thousands of biomolecules organize into multiple coexisting liquid-like phases that enable diverse functions. Despite their ubiquity in nature and industry, how numerous interactions between components encode their macroscopic multiphase behavior remains poorly understood. We employ statistical physics approaches to reveal the emergent dynamical, compositional, and steady-state properties of coexisting phases in fluid mixtures with many randomly interacting components. Building on these findings, we demonstrate design strategies to encode linear or nonmonotonic scaling relationships between the number of phases and components and suggest active routes to tunably modify multiphase coexistence.

Author contributions: K.S. and M.P.B. designed research; K.S. performed research; K.S. analyzed data; and K.S. and M.P.B. wrote the paper.

The authors declare no competing interest.

This article is a PNAS Direct Submission. A.K. is a guest editor invited by the Editorial Board.

[1]To whom correspondence may be addressed. Email: krishnashrinivas@g.harvard.edu.

This article contains supporting information online at http://www.pnas.org/lookup/suppl/doi:10.1073/pnas.2108551118/-/DCSupplemental.

Published November 1, 2021.

Here, we develop a dynamic model of phase separation in fluid mixtures with many randomly interacting components. Through simulation of the model, we demonstrate that fluid mixtures with many components exhibit characteristic similarities in phase-separation kinetics and in the number and compositional features of coexisting phases at steady state, even when the underlying interactions are random. We propose a simple model, combining insights from random-matrix theory and dynamical systems analyses, that predicts dynamical and steady-state characteristics of the emergent phase behavior. We subsequently discuss two distinct ensembles (or component design strategies) that encode either linear or nonmonotonic scaling (i.e., with an optima) between the number of coexisting phases and components. Finally, we extend our framework to incorporate chemical reactions and show that active turnover of components can tunably modulate the number of coexisting phases at steady state even without altering overall fluid composition. Overall, our model provides a framework to predict and design emergent multiphase kinetics, compositions, and steady-state properties in fluid mixtures with many interacting components.

Results

Model Definition. We begin by describing the free energy (f) of a mixture of $(N+1)$ interacting species through a mean-field regular solution model at fixed temperature and overall volume (Eq. **1**). Here, ϕ_i represents the volume fraction of each species i, and $\phi_s = 1 - \sum_i \phi_i$ is the volume fraction of the remaining component, which is typically the solvent. Equivalently, this model can also represent the normalized volume fractions of $(N+1)$ components in a solution where the total solute concentration is invariant across phases. χ_{ij} and χ_{is} are the effective pairwise interactions among different species and between components and solvent, respectively. For simplicity, we assume an initially uniform solute mixture ($\phi_i = \frac{\beta}{N}\ \forall i,\ \phi_s = 1-\beta; \beta$ is total solute volume fraction), inert solvent ($\chi_{is} \approx 0$), and components that do not self-interact [i.e., χ_{ij} only depends on interaction energy (ϵ_{ij}) between components $i,j, i \neq j$]. Further, we stipulate that the pairwise interactions χ_{ij} are independent random variables, which are drawn from a distribution with finite mean ν and variance σ^2 (Fig. 1*A*):

$$f = \sum_{i=1}^{N} \phi_i \log(\phi_i) + \frac{1}{2}\sum_{i=1}^{N}\sum_{j=1}^{N} \chi_{ij}\phi_i\phi_j + \phi_s \log(\phi_s) + \sum_{i=1}^{N} \chi_{is}\phi_i\phi_s \qquad [1]$$

$$J_{ij} = \frac{\partial^2 (f)}{\partial \phi_i \partial \phi_j} = \frac{\delta_{ij}}{\phi_i} + \frac{1}{\phi_s} + \chi_{ij};\ J = \frac{N}{\beta}\bar{\bar{I}} + \bar{\bar{\chi}}_{eff}. \qquad [2]$$

The point beyond which a mixture spontaneously phase separates—the spinodal or the marginally stable state—occurs when the minimum eigenvalue λ_{min} of the Hessian matrix J (Eq. **2** and *SI Appendix*) crosses zero [i.e., $\lambda_{min}(J) = 0$]. The corresponding eigenvector gives the initial direction of instability (*SI Appendix*, Fig. S1), which leads to either condensation-type ($\nu \leq -N$) or demixing-type instabilities ($\nu \geq -\frac{2\sigma}{\sqrt{N}} - \frac{1}{1-\beta}, 0; \sigma > \frac{\sqrt{N}}{2\beta}$) depending on the values of ν, σ (29, 34). During condensation, the instability points toward dilute and dense phases with similar compositions since individual components are strongly attractive on average, as determined from the angle between the marginal eigenvector and the initial composition being close to 0 or 180 (*SI Appendix*, Fig. S1*C*). Conversely, during demixing, the initial instability, whose direction is roughly perpendicular to the uniform mixture (*SI Appendix*, Fig. S1*C*), points to phases with distinct compositions. In general, solutions that demix contain unstable modes beyond the marginally stable point, potentially leading to multiphase coexistence. Multiphase coexistence does not generically occur in condensation transitions because of the band gap between the smallest eigenvalue and the rest of the spectra (*SI Appendix*, Fig. S1). Motivated by this, here we focus on phase separation in solutions whose component interactions are variable but not strongly attractive on average ($\nu \approx 0,\ \sigma > \frac{\sqrt{N}}{2\beta}$).

After the initial instability, fluid mixtures undergoing spinodal decomposition display rich dynamics and diverse multiphase coexistence (Fig. 1*A*). To probe the kinetics and emergent steady-state properties, we formulate a set of dynamical equations to track the evolution of N-independent volume fractions [$\phi_i(\vec{r}, t),\ i = 1....,N$] (Eq. **3**). The temporal evolution of a component's volume fraction [$\phi_i(\vec{r}, t)$] depends on diffusive fluxes driven by gradients of chemical potential $\mu_i(\{\phi_j\} = \frac{df}{d\phi_i})$ with a mobility coefficient M_i, also known as conserved model B dynamics (35, 36). We assume that all components obey $M_i = M\phi_i$, approximately recapitulating Fickian diffusion in the limit of noninteracting, dilute components (*SI Appendix*). Finally, we include surface-tension effects ensuring long-wavelength stability by modifying the bulk chemical potentials with a component-independent gradient term ($\mu_i = \frac{df}{d\phi_i} - \kappa\nabla^2\phi_i$):

$$\frac{\partial \phi_i(\vec{r}, t)}{\partial t} = \vec{\nabla}.\left(M_i \nabla \mu_i\left(\{\phi_j(\vec{r}, t)\}\right)\right). \qquad [3]$$

We numerically simulate these nonlinear, coupled partial differential equations using Fourier space representations to compute gradients and fluxes (*SI Appendix*). Unless specified otherwise, a two-dimensional grid ($L \times L, L = 64$) is initialized with a uniform and equimolar solution ($\phi_i = \frac{1}{N+1}; \beta = \frac{N}{N+1}$) with small compositional fluctuations. For each simulation, we sample the interaction matrix χ from a normal distribution (Fig. 1*A*) with zero mean and specified variance (quenched disorder). At any time point, the state of the system is described by the volume-fraction tensor ($N \times L \times L$), giving the volume fraction of each component at every point in space. We can infer the number of phases N_{ph} by performing principal component analysis (PCA) on this matrix after flattening the tensor along the spatial dimensions and filtering out interfaces between phases that vary in composition. We then identify the significant eigenvalues that correspond to individual phases (Fig. 1*B* and *SI Appendix*). We identify which phase each point in space belongs to by first performing K-means clustering (with the number of clusters as the number of phases from PCA) followed by classification to assign individual points to the closest phase by composition $\vec{\phi}_{N\times 1}(\vec{r}; \gamma - phase)$. For all the points assigned to a phase, we compute spatially averaged volume fractions that characterize the bulk composition of the γ phase $\vec{\phi}\ (\vec{r}\ )_\gamma$ (*SI Appendix*). These approaches enable us to characterize the spatiotemporal evolution and steady-state properties of fluid mixtures that undergo phase separation through spinodal decomposition.

Multiple Phases with Distinct Compositions Characterize Random Fluid Mixtures. To explore phase behavior of multicomponent solutions, we first simulate the dynamics of an initially equimolar solution of $N = 16$ components (labeled ϕ_i) whose pairwise interactions are randomly sampled from $\chi_{ij} \sim Normal(0, \sigma = 4.8)$. This choice of parameters ensures spontaneous phase separation with multiple initial unstable modes. At steady state, the mixture exhibits heterogeneous, multiphase coexistence (Fig. 1*C*). The steady-state solution has four coexisting phases (Fig. 1*D*) that are enriched in a distinct, yet characteristic number of components per phase (Fig. 1*E* and *SI Appendix*). Such multiphase coexistence with differing compositions occurs generically for different choices of parameters (*SI Appendix*, Fig. S2).

A key question is to understand how the steady-state properties of the phases relate to the interaction distribution between components. To explore this, we ran many simulations under identical

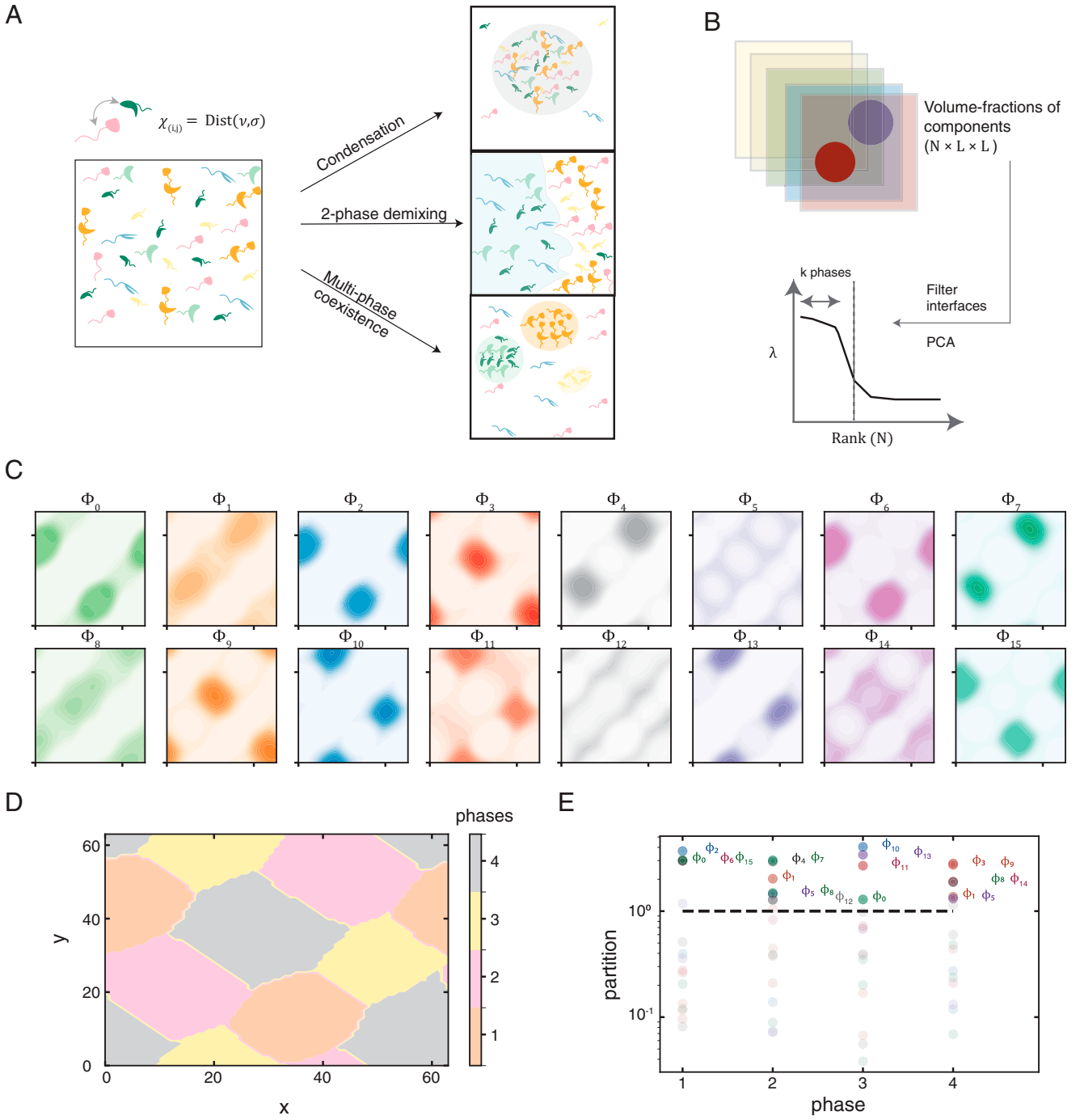

Fig. 1. A model for phase separation in multicomponent fluid mixtures. (*A*) A schematic depicting that the interactions between pairs of components are randomly drawn from a distribution and encode varying emergent properties. (*B*) Schematic depicting postprocessing analyses on simulation data to identify the coexisting phases from PCA. (*C*) Plots depict volume-fraction profiles of 16 components (labeled $\phi 0$ to $\phi 15$) at steady state from a single trajectory with identical color-bar scales (0, 0.75). Darker colors represent regions of higher volume fraction, and simulation parameters are presented in the text and *SI Appendix*. (*D*) The different phases (labeled one to four) present at steady state in *A* are depicted here. (*E*) The partition ratio (the ratio of the average volume fraction in a phase over the total initial volume fraction) of all components is plotted for each phase (*x* axis) at steady-state conditions shown in *A*. The highlighted components are enriched in those respective phases, and the dashed line represents no enrichment (partition = 1).

conditions while resampling from the interaction matrix specified above. Although the precise values of steady-state compositions vary between different simulations, there were striking statistical similarities between both the number of distinct phases at steady state and the temporal dynamics leading to this steady state (in Fig. 2*A*, the green line is the trajectory in Fig. 1 *C*–*E*). This statistical convergence in the expected number of coexisting phases is independent of the choice of mobility parameter (*SI Appendix*, Fig. S3*B*), simulation length (*SI Appendix*, Fig. S3*C*), or specific simulation parameters (*SI Appendix*, Fig. S3*D*).

The compositions of the steady-state phases also exhibit similarities. To characterize the compositions at steady state, we compute the angle (Fig. 2*B*) between compositions of the pairs of coexisting phases $(\theta_{\alpha\beta})$ and also measure the number of

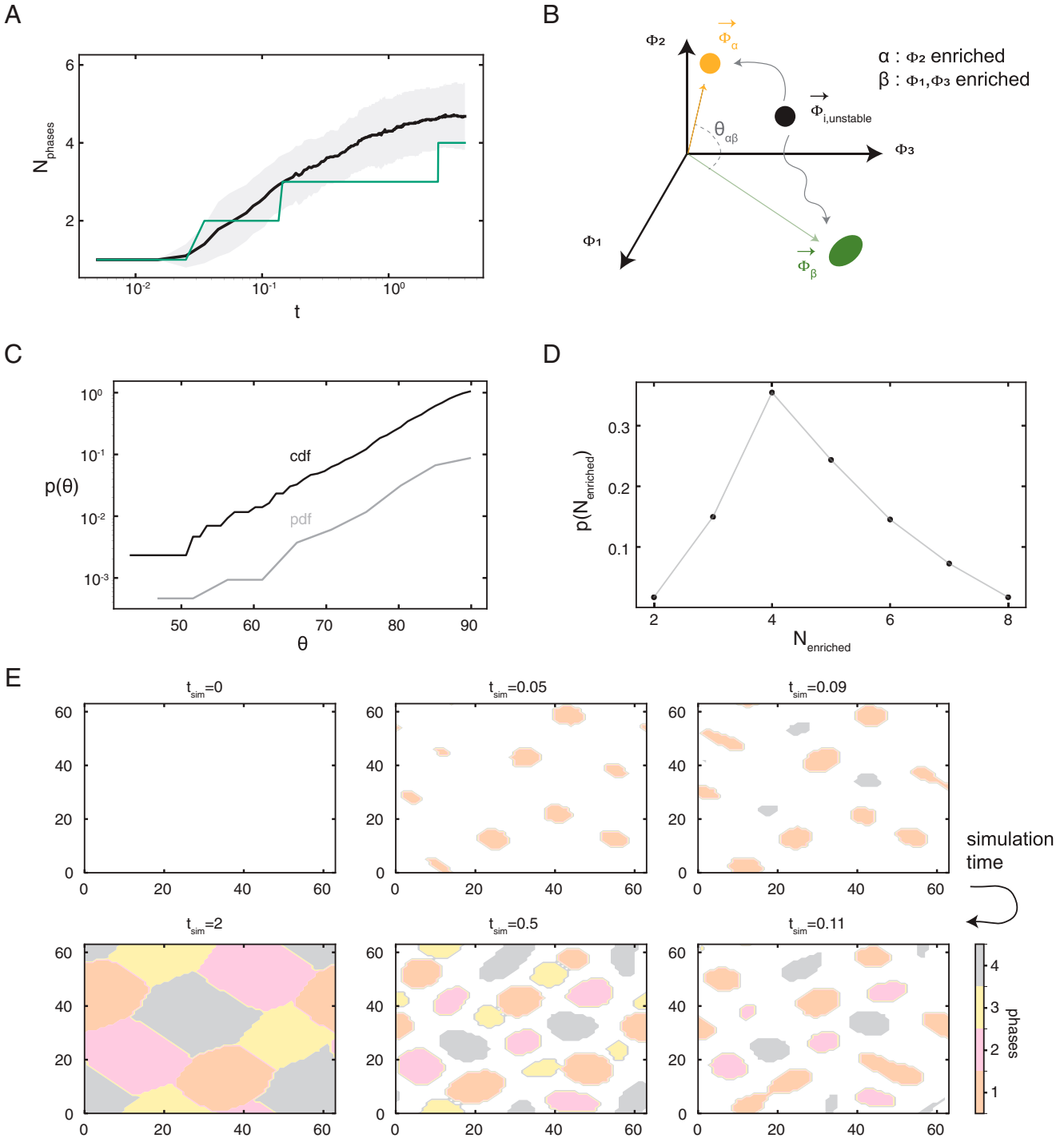

Fig. 2. Multiple phases with distinct compositions characterize random fluid mixtures. (*A*) Number of coexisting phase (*y* axis) versus simulation time (*x* axis, log scale) for simulations with $n = 16$, $\chi \sim N(0, \sigma = 4.8)$ (the same conditions as in Fig. 1*C*). The solid line represents the mean of 50 different trajectories, the filled regions represent one SD, and the green line represents the specific trajectory whose steady-state properties are shown in Fig. 1 *C*–*E*. (*B*) A schematic illustrating how compositional observables are computed from steady-state compositions [i.e., the angle between coexisting phases (θ)] and the number of enriched components per phase are computed. In the example, an initially unstable phase of three components demixes to form two phases (α, β) that are enriched in a distinct number of components (shown in the legend). (*C*) Probability distribution function (pdf) and cumulative distribution function (cdf) of angles between coexisting phases at steady state for simulation parameters in *A*. (*D*) Probability ($p_{N_{enr}}$) distribution of the number of enriched components (*x* axis, N_{enr}) per phase at steady state for simulation parameters in *A*. (*E*) Individual snapshots of the simulation trajectory reported in Fig. 1*C* labeled with existing phases (one to four from steady state, white or unlabeled if like the initial equimolar solution). The steady-state labels are shown in the color bar, whose bulk compositions are used to assign phase labels at earlier times (*SI Appendix*).

components enriched in each particular phase ($N_{enriched}$). Phases with $\theta_{\alpha\beta}$ close to zero have largely similar compositions, whereas those close to $\pi/2$ are enriched in different sets of components. Fig. 2*C* shows the distribution $p(\theta_{\alpha\beta})$ calculated across multiple simulations, demonstrating that different phases have composition vectors that are largely orthogonal, with an

exponential decay in the probability of phases being more similar by composition. Since individual concentrations must be positive and obey overall mass balance, this indicates that coexisting phases are mostly enriched in distinct sets of components. The number of enriched components per phase $p(N_{enriched})$ is distributed around values of $N_{enriched} = 3, 4, 5$ (Fig. 2*D*). This is consistent with the distinct phases being orthogonal in component partitioning $< N_{enriched} > \approx \frac{N+1}{<_{phases}>} \sim 4$. This observed compositional orthogonality is independent of the specific simulation parameters (*SI Appendix*, Fig. S3 *E* and *F*). Overall, the steady-state phase behavior of random fluid mixtures is characterized by multiple coexisting phases with distinct compositions.

A Simple Random Matrix–Derived Theory Predicts Steady-State Phase Behavior of Fluid Mixtures. The consistency in dynamic and steady-state properties of random mixtures motivated us to explore whether we could unify the emergent phase behavior through a theoretical framework. First, we asked whether the steady-state multiphase coexistence was related to the properties of the initially uniform mixture, as characterized by the Hessian of the free energy. We ran simulations across several conditions (varying σ, N) and computed both the number of unstable modes at the beginning of each trajectory ($N_{\lambda<0}$ is the number of negative eigenvalues from linear stability analyses) (*SI Appendix*) as well as the number of coexisting phases at steady state (N_{ph}). Strikingly, when examined across simulations with diverse parameters, these exhibited a linear relation where $N_{ph} \approx N_{\lambda<0} + 1$ (Fig. 3*A*). This implies that each linearized unstable eigenmode typically gives rise to a unique coexisting phase at steady state (*SI Appendix*). We note that this relation is statistical in nature (i.e., for a given number of unstable modes, there exists a distribution of the number of observed phases that is strongly concentrated at $N_{ph} \approx N_{\lambda<0} + 1$, with small nonzero probabilities of observing more or fewer phases). Since the eigenvectors corresponding to these initial unstable modes are largely perpendicular to each other (*SI Appendix*, Fig. S4*A*), this may contribute to the observed compositional orthogonality between coexisting phases at steady state (Fig. 2*C* and *SI Appendix*, Fig. S3*E*). Overall, our results suggest that the number of coexisting phases at steady state in fluid mixtures undergoing phase separation by spinodal decomposition can be computed by simply computing the number of unstable modes in the uniform mixture. This is a striking conclusion because in general, the number of stable states in a nonlinear free energy functional is independent of the number of unstable modes in the initial dynamics.

The number of unstable modes or negative eigenvalues can be counted using Wigner's semicircle law for random matrices, giving $< N_{ph} > = N \times F_{2\sigma\sqrt{N}}\left(\lambda \leq -\frac{N}{\beta}\right) + 1$ (*SI Appendix*). Here, F is the cumulative distribution function (cdf) of the semicircle distribution whose eigenvalues are between $\pm 2\sigma\sqrt{N}$, and the argument is the entropic cost that needs to be offset to phase separate (*SI Appendix*). Since the eigenvalues of the semicircle distribution are equally spaced on average, the number of phases can be approximated as

$$N_{phases} \approx \frac{N\left(1 - \frac{\sqrt{N}}{2\beta\sigma}\right) + 1}{2}. \qquad [4]$$

Eq. **4** implies that when $\sigma = \alpha\sqrt{N}$, the number of phases scales linearly with the number of components. In the next section, we will discuss a biophysical interpretation of the proportionality constant α. When $\sigma < \frac{\sqrt{N}}{2\beta}$, there are no unstable modes, and the uniform phase remains stable, as expected. If the interactions between species are strongly variable ($\sigma \gg \sqrt{N}$), Eq. **4** implies a maximum of $\frac{N+1}{2}$ coexisting phases at steady state. Interestingly, this asymptotic scaling is significantly less than the upper constraint of $N + 2$ (or N if temperature and pressure/volume are fixed) originally formulated by Gibbs (16). Note that this asymptotic scaling of $N/2$ likely arises from the competing network of interactions between components and should be expected to hold even when the average of the interaction distribution, ν, is nonzero, which at most, adds only one single orthogonal eigenmode (*SI Appendix*).

After the initial instability, linear stability analyses predict that each unstable mode grows exponentially ($\exp - a\lambda t$) (*SI Appendix*), so the characteristic time for a phase to form scales as $t_{ph} \propto 1/\lambda$. Since the unstable eigenvalues are equally spaced on average ($\lambda_{min} = \lambda_1 < \lambda_2 < ... < \lambda_k < ... < \lambda_\gamma < 0\ s.t.\ \lambda_k - \lambda_{k+1} = constant$), the typical time for the kth phase to macroscopically form is larger for higher k in $t_{ph=k} \propto \frac{-1}{<\lambda_k>}$ (the proportionality constant can be approximately estimated) (*SI Appendix*). This relation, although an approximation, predicts multistaged phase-separation kinetics; newer phases macroscopically emerge at later times in a sequential order—predictions that are consistent with observations (Figs. 2*A* and 3*D* and *SI Appendix*, Fig. S4*B*). This is made vivid by tracking the temporal evolution of different phases for the example trajectory shown in Fig. 1*C* (Fig. 2*E* and *SI Appendix*). Statistical analyses of multiple trajectories (*SI Appendix*) confirm that most phases (>99%) demix from the initially unstable phase, albeit at different times, but do not rule out the possibility that on rare occasions (<1%), phases may emerge by demixing from other coexisting phases (*SI Appendix*, Fig. S4*C*). Together, these results support a model derived from random-matrix theory that connects statistical properties of the initially homogeneous solution to the dynamics, compositional features, and number of steady-state phases in fluid mixtures with randomly interacting components.

A Simple Model Predicts Steady-State Behavior of Random Mixtures from Different Ensembles. We next sought to explore whether we could identify ensembles that connect microscopic parameters to different emergent phase behavior—including by varying number of species (N), mole fraction (β), or the shape of the interaction distribution. In particular, Eq. **4** suggests that scaling the variance with the number of components, namely $\sigma = \sigma(N) \propto N^{1/2}$ [i.e., $\sigma = \alpha N^{1/2}\ (\alpha - ensemble)$], should lead to linear encoding between the number of steady-state phases and components.

To probe this more thoroughly, we ran simulations across a wide range of (N, α, σ). In the α-ensemble, the predicted scaling of number of coexisting phases from Eq. **4** scales linearly with N and saturates with increasing α, in agreement with theoretical predictions (Fig. 3 *C* and *D*). By contrast, in the constant σ-ensemble, theory predicts an optimal number of components that maximizes the number of coexisting phases at steady state [$N^{opt}_{components} \approx \left(\frac{4}{3}\sigma\right)^2$] (*SI Appendix*), which broadly agrees with simulation predictions (Fig. 3 *E* and *F*). Intuitively, with fewer components, phase separation is promoted due to lower entropic costs, but the maximum number of coexisting phases is bounded by $\frac{N+1}{2}$. Conversely, in the limit of many components, the system is stable and does not phase separate (entropic stabilization $\propto N$, whereas enthalpic terms scale as $\sigma\sqrt{N}$), thus leading to nonmonotonic scaling. In all cases, the predictions deviate from simulation at either low N or σ, when fluctuations in the unstable modes of the eigenspectra are of order unity. Theoretical corrections based on Tracy–Widom extreme-value statistics reduce the gap between theory and simulation, particularly at low N, σ (*SI Appendix*, Fig. S5*A*). Finally, simulations match theory for equimolar solutes with lower total solute volume fractions (lower β) (*SI Appendix*, Fig. S5*B*), and theoretical predictions continue to exhibit similar scaling relationships (*SI Appendix*, Figs. S5 *C–F*) in regimes where simulations are numerically inaccessible ($\alpha \gg 1, \sigma \gg \sqrt{N}$). These results show that increasing the variance of interactions proportionally with the number of components

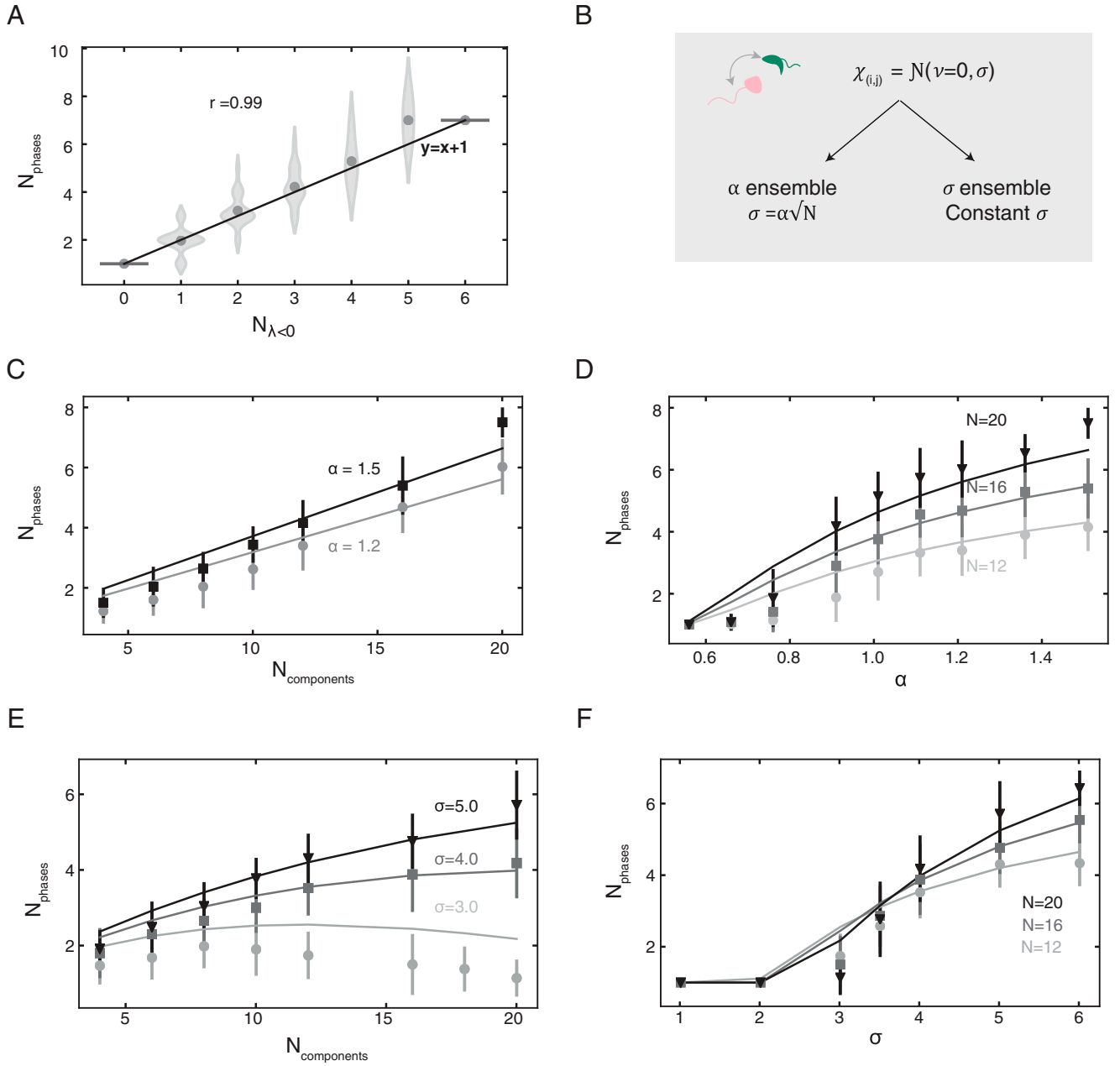

Fig. 3. A simple scaling predicts steady-state behavior of random mixtures from different ensembles. (*A*) The number of phases at steady state (*y* axis) versus the number of negative eigenvalues of the initial equimolar mixture. Histograms represent simulation results that are collapsed from a range of different N, σ, and the solid line represent the equation $y = x + 1$. The correlation coefficient is reported between the mean of simulation results and the solid line. (*B*) A schematic depicting the two interaction ensembles with different variance scaling. The α-ensemble consists of components whose variance in interactions scales with the number of distinct species, and the σ-ensemble has a distribution of fixed variance. (*C* and *D*) Variation of the number of coexisting phases at steady state with the number of components (linear scaling) and different values of α (monotonic saturation) in the α-ensemble. Solid lines represent theoretical predictions based on the Wigner formula, dots represent the mean of simulation results, and vertical dashes represent one SD around the mean. In each plot, darker lines represent higher values of α and *N*, and different marker types are employed to reinforce this. (*E* and *F*) Variation of the number of coexisting phases at steady state with the number of components (nonmonotonic) and different values of σ (monotonic saturation) in the fixed σ-ensemble. Solid lines represent theoretical predictions based on the Wigner formula, dots represent the mean of simulation results, and vertical dashes represent one SD around the mean. In each plot, darker lines represent higher values of σ and *N*, and different marker types are employed to reinforce this.

(for example, by increasing the number of interactions sites) allows for encoding more phases. Conversely, sampling more components from a distribution of fixed variance (for example, all components have the same number of interaction sites) has a maximal number of coexisting phases.

Active Turnover of Components Modulates the Number of Coexisting Phases at Steady State. In most biological systems, interacting components are actively being produced and degraded (37). To study how such chemical reactions impact phase behavior, we modify our dynamical equations to

$$\frac{d\phi_i}{dt} = \vec{\nabla}\cdot\left(M_i\,\vec{\nabla}\mu_i\right) + \sum_j r_{ij}, \qquad [5]$$

where r_{ij} are sets of reactions ($\{j\}$) that change the fluxes of species i. In the simplest case of turnover, each component is produced at fixed rate k and degraded at rate $k_{off} = kN/\beta$. In the absence of phase separation, each component's steady-state volume fraction is $\phi_i^{ss} = \frac{k_{on}}{k_{off}} = \frac{\beta}{N}$. As before, when $\beta = \frac{N}{N+1}$, this corresponds to an equimolar solution [i.e., $\phi_i^{ss} = 1/(N+1)$].

We then perform linear stability analyses (*SI Appendix*), which show that phase separation is suppressed by high rates of turnover (i.e., larger values of k_{off}), consistent with previous theoretical work in binary or ternary mixtures (19, 24). Active turnover effectively introduces local mixing by cyclically synthesizing and degrading components, which counteract spatial variations that arise from phase separation. When the rate of turnover becomes dominant to induce mixing at large length scales, it effectively decreases the band of unstable eigenvalues that contribute to phase separation. The unstable eigenvalues that continue to persist are orthogonal to each other and should continue to drive multiphase coexistence, albeit with lower numbers of steady-state phases. More generally, the higher the rate of turnover, the lower the number of steady-state phases (*SI Appendix*). Further, our theory predicts that the number of coexisting phases at steady state can be tunably suppressed by varying the absolute rates of turnover (k_{on}, k_{off}), even when keeping their ratio constant (i.e., the overall fluid composition at steady state remains equimolar and identical to the initial conditions, with a scaling of $n^{ss}_{phases,k} - n_{phases,k=0} \propto -\frac{k\sqrt{N}}{\sigma}$) (*SI Appendix*). To test this hypothesis, we ran simulations in which we varied the rate of turnover while keeping their ratio constant (increasing both k_{on}, k_{off} for all components) and averaged observables across replicate trajectories. We find that increasing rates of active turnover leads to a decreasing number of coexisting phases (Fig. 4*A*), and simulations largely correlate with the simple theoretical prediction (Fig. 4*B*). Replacing the linearized approximation with the nonlinear Wigner cdf (*SI Appendix*) provides substantially better agreement between theory and simulation (Fig. 4*B*, green line). Overall, this suggests that active turnover of components can serve as a route to tunably modulate multiphase coexistence in random fluids even without altering the relative or overall composition of such mixtures.

Discussion

Over the past several years, there has been a growing appreciation of the role of multicomponent and coexisting phases inside a cell. These phases, or condensates, compartmentalize many interacting species and pathways to enable diverse yet specific functions across cell types and organisms. More generally, fluid mixtures with many phases and components are prevalent in biology, soft matter, and industry. Yet, we still do not understand how numerous interacting components encode the emergent multiphase behavior. The goal of this study is to develop a simple model of the dynamics and steady-state phase behavior in fluid mixtures with many components. We choose the interactions between components from an underlying distribution and thereby, can use random-matrix theory to analyze the resulting dynamics. Through simulation and theory, we find that spontaneous phase separation of such mixtures is characterized by staged phase-separation dynamics and multiple coexisting phases at steady state with distinct nonoverlapping compositions. Importantly, our model suggests that these characteristics do not require fine-tuning of composition or interaction parameters; rather, they are an emergent property of fluid mixtures with many components with random interactions. Whether staged phase-separation kinetics is common to or relevant in biological systems remains unexplored but may be a potential mechanism to temporally orchestrate biochemical pathways. Subsequently, we design different component ensembles that encode linear or optimal scaling of the number of coexisting phases versus components, which we validate through simulation and random-matrix theory. Strikingly, we identify an upper bound for the maximum number of coexisting phases in random mixtures, derived from dynamical considerations, that is asymptotically lower than the Gibbs phase rule. Random interactions effectively introduce competing interaction networks, which likely limit the maximal number of possible coexisting phases. Motivated by the observation that biological fluids often exhibit component turnover such as synthesis/degradation of biomolecules, we show that active turnover of components can tunably modify steady-state multiphase coexistence, even without altering overall fluid composition. An exciting next step will be to characterize how reaction networks that exhibit complex topology and spatial features influence phase behavior in multicomponent mixtures, building on ideas initially introduced for two- or three-component fluids (19, 25).

The model formulated herein is only the first step in being able to design multicomponent phases in terms of their individual components. Recently, there has been tremendous progress in characterizing the sequence to the phase-behavior relationship of individual proteins and nucleic acids (14, 26, 38), composition of different condensates (39–41),

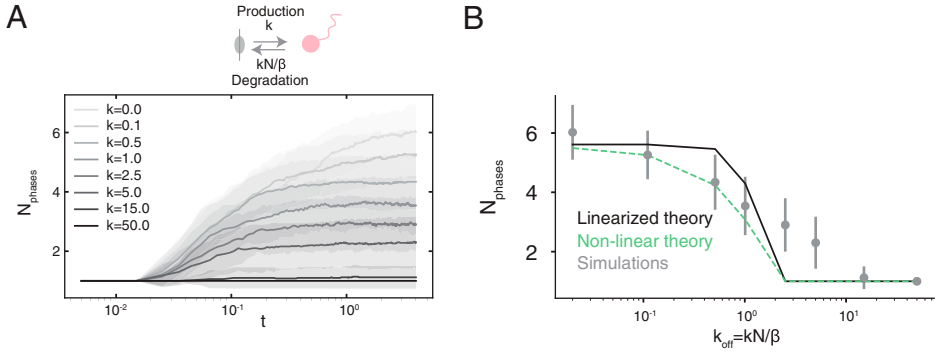

Fig. 4. Active species turnover tunably modulates multiphase coexistence at steady state. (*A*) The schematic depicts constant production and first-order degradation of components. The graph shows the number of phases versus simulation time (in log scale) across a range of reaction rates in a system with $N = 20$ components and $\sigma = 5.4$. Solid lines represent the mean of trajectories (>40 replicates per condition), shaded bars represent one SD on each side of the mean, and darker lines corresponds to faster rates of turnover. (*B*) Simulation (dots) and theoretical predictions (solid line) based on the linearized model on the number of coexisting phases at steady state versus the rate of turnover. The green line is derived from the nonlinear theoretical model (*SI Appendix*). Solid circles represent the mean number of coexisting phases, and vertical lines represent one-SD ranges under the same parameter conditions as above.

and regulated formation of condensates at specific locations, often through nucleation (42, 43). Soft matter colloidal systems (44, 45), DNA-based nanotechnology (12, 46), programmable magnetic materials (47), and multiplexed protein design offer diverse attractive routes to both experimentally test predictions and serve as platforms to enable design of multiphase fluid mixtures. While our numerical model is focused on characterizing spinodal decomposition of equimolar fluid mixtures, extensions to larger systems (N ? 20) with varying composition and incorporation of approaches to study nucleation dynamics, including recent graph theory–based models (48), will facilitate programmable design of equilibrium multiphase coexistence. An important related problem is the design of targeted multiphase mixtures whose compositions and interactions are specifically tuned, not random. Computational and theoretical approaches for programming phase behavior in these systems will enable material design using synthetic and biological constituents. Another exciting direction is to incorporate energy-consuming processes as part of the design. Examples include nonreciprocal interactions, chemical reaction networks, molecular motors, and motile particles—all of which are characteristic of living systems. More generally, studying the interplay of nonequilibrium processes and multiphase behavior in fluid mixtures will be an exciting and rich area for biology and soft matter physics.

Materials

Phase-field simulations and subsequent data analyses were performed using custom code written in python. We employ the results from random-matrix theory and dynamical systems analyses in deriving the theoretical scaling relationships presented in the text. More details about theory, simulation, and numerical methods for postprocessing are available in *SI Appendix*.

Data Availability. Code has been deposited in GitHub (https://github.com/krishna-shrinivas/2021_Shrinivas_Brenner_random_multiphase_fluids).

ACKNOWLEDGMENTS. We thank Ofer Kimchi, Ella King, Jon Henninger, and members of the laboratory of M.P.B. for helpful discussions. We also thank the reviewers for their expertise and feedback, which improved our study. K.S. was supported by NSF–Simons Center for Mathematical and Statistical Analysis of Biology at Harvard Award 1764269 and the Harvard Faculty of Arts and Sciences Quantitative Biology Initiative. M.P.B. was supported by Office of Naval Research Grant N00014-17-1-3029 and the Simons Foundation.

1. Y. Shin, C. P. Brangwynne, Liquid phase condensation in cell physiology and disease. *Science* **357**, eaaf4382 (2017).
2. S. F. Banani, H. O. Lee, A. A. Hyman, M. K. Rosen, Biomolecular condensates: Organizers of cellular biochemistry. *Nat. Rev. Mol. Cell Biol.* **18**, 285–298 (2017).
3. A. S. Lyon, W. B. Peeples, M. K. Rosen, A framework for understanding the functions of biomolecular condensates across scales. *Nat. Rev. Mol. Cell Biol.* **22**, 215–235 (2020).
4. S. Alberti, A. A. Hyman, Biomolecular condensates at the nexus of cellular stress, protein aggregation disease and ageing. *Nat. Rev. Mol. Cell Biol.* **22**, 196–213 (2021).
5. J. Berry, S. C. Weber, N. Vaidya, M. Haataja, C. P. Brangwynne, RNA transcription modulates phase transition-driven nuclear body assembly. *Proc. Natl. Acad. Sci. U.S.A.* **112**, E5237–E5245 (2015).
6. J. Kirschbaum, D. Zwicker, Controlling biomolecular condensates via chemical reactions. *J. R. Soc. Interface* **18**, 20210255 (2021).
7. M. Feric *et al.*, Coexisting liquid phases underlie nucleolar subcompartments. *Cell* **165**, 1686–1697 (2016).
8. A. A. Deniz, Networking and dynamic switches in biological condensates. *Cell* **181**, 228–230 (2020).
9. A. I. Curatolo *et al.*, Cooperative pattern formation in multi-component bacterial systems through reciprocal motility regulation. *Nat. Phys.* **16**, 1152–1157 (2020).
10. J. Agudo-Canalejo, R. Golestanian, Active phase separation in mixtures of chemically interacting particles. *Phys. Rev. Lett.* **123**, 018101 (2019).
11. A. Giometto, D. R. Nelson, A. W. Murray, Antagonism between killer yeast strains as an experimental model for biological nucleation dynamics. *bioRxiv* [Preprint] (2020). https://www.biorxiv.org/content/10.1101/2020.09.08.288423v1 (Accessed 15 April 2021).
12. L. Di Michele *et al.*, Multistep kinetic self-assembly of DNA-coated colloids. *Nat. Commun.* **4**, 2007 (2013).
13. N. Asherie, A. Lomakin, G. B. Benedek, Phase diagram of colloidal solutions. *Phys. Rev. Lett.* **77**, 4832–4835 (1996).
14. J. R. Simon, N. J. Carroll, M. Rubinstein, A. Chilkoti, G. P. López, Programming molecular self-assembly of intrinsically disordered proteins containing sequences of low complexity. *Nat. Chem.* **9**, 509–515 (2017).
15. T. Kaur *et al.*, Sequence-encoded and composition-dependent protein-RNA interactions control multiphasic condensate morphologies. *Nat. Commun.* **12**, 872 (2021).
16. J. W. Gibbs, On the Equilibrium of Heterogeneous Substances. Amer. Jour. Sci. **3.96**, *441–458* (1878).
17. P. J. Flory, Thermodynamics of high polymer solutions. *J. Chem. Phys.* **10**, 51–61 (1942).
18. M. L. Huggins, Solutions of long chain compounds. *J. Chem. Phys.* **9**, 440 (1941).
19. S. C. Glotzer, D. Stauffer, N. Jan, Monte Carlo simulations of phase separation in chemically reactive binary mixtures. *Phys. Rev. Lett.* **72**, 4109–4112 (1994).
20. J. Wolff, C. M. Marques, F. Thalmann, Thermodynamic approach to phase coexistence in ternary phospholipid-cholesterol mixtures. *Phys. Rev. Lett.* **106**, 128104 (2011).
21. J. T. G. Overbeek, M. J. Voorn, Phase separation in polyelectrolyte solutions; theory of complex coacervation. *J. Cell. Physiol. Suppl.* **49** (suppl. 1), 7–22 (1957).
22. S. Mao, D. Kuldinow, M. P. Haataja, A. Košmrlj, Phase behavior and morphology of multicomponent liquid mixtures. *Soft Matter* **15**, 1297–1311 (2019).
23. S. Mao, M. S. Chakraverti-Wuerthwein, H. Gaudio, A. Košmrlj, Designing the morphology of separated phases in multicomponent liquid mixtures. *Phys. Rev. Lett.* **125**, 218003 (2020).
24. D. Zwicker, A. A. Hyman, F. Jülicher, Suppression of Ostwald ripening in active emulsions. *Phys. Rev. E Stat. Nonlin. Soft Matter Phys.* **92**, 012317 (2015).
25. C. A. Weber, D. Zwicker, F. Jülicher, C. F. Lee, Physics of active emulsions. *Rep. Prog. Phys.* **82**, 064601 (2019).
26. J. Wang *et al.*, A molecular grammar governing the driving forces for phase separation of prion-like RNA binding proteins. *Cell* **174**, 688–699.e16 (2018).
27. E. W. Martin *et al.*, Valence and patterning of aromatic residues determine the phase behavior of prion-like domains. *Science* **367**, 694–699 (2020).
28. P. Sollich, M. E. Cates, Projected free energies for polydisperse phase equilibria. *Phys. Rev. Lett.* **80**, 1365–1368 (1998).
29. R. P. Sear, J. A. Cuesta, Instabilities in complex mixtures with a large number of components. *Phys. Rev. Lett.* **91**, 245701 (2003).
30. E. P. Wigner, On the statistical distribution of the widths and spacings of nuclear resonance levels. *Math. Proc. Camb. Philos. Soc.* **47**, 790–798 (1951).
31. V. Dahirel *et al.*, Coordinate linkage of HIV evolution reveals regions of immunological vulnerability. *Proc. Natl. Acad. Sci. U.S.A.* **108**, 11530–11535 (2011).
32. M. Nitzan, M. P. Brenner, Revealing lineage-related signals in single-cell gene expression using random matrix theory. *Proc. Natl. Acad. Sci. U.S.A.* **118**, e1913931118 (2021).
33. R. M. May, Will a large complex system be stable? *Nature* **238**, 413–414 (1972).
34. W. M. Jacobs, D. Frenkel, Phase transitions in biological systems with many components. *Biophys. J.* **112**, 683–691 (2017).
35. M. Kardar, *Statistical Physics of Fields* (Cambridge University Press, Cambridge, United Kingdom, 2007).
36. P. C. Hohenberg, B. I. Halperin, Theory of dynamic critical phenomena. *Rev. Mod. Phys.* **49**, 435–479 (1977).
37. S. B. Cambridge *et al.*, Systems-wide proteomic analysis in mammalian cells reveals conserved, functional protein turnover. *J. Proteome Res.* **10**, 5275–5284 (2011).
38. W. Zheng, G. Dignon, M. Brown, Y. C. Kim, J. Mittal, Hydropathy patterning complements charge patterning to describe conformational preferences of disordered proteins. *J. Phys. Chem. Lett.* **11**, 3408–3415 (2020).
39. D. W. Sanders *et al.*, Competing protein-RNA interaction networks control multiphase intracellular organization. *Cell* **181**, 306–324.e28 (2020).
40. J. A. Riback *et al.*, Composition-dependent thermodynamics of intracellular phase separation. *Nature* **581**, 209–214 (2020).
41. J. Fei *et al.*, Quantitative analysis of multilayer organization of proteins and RNA in nuclear speckles at super resolution. *J. Cell Sci.* **130**, 4180–4192 (2017).
42. D. Hnisz, K. Shrinivas, R. A. Young, A. K. Chakraborty, P. A. Sharp, A phase separation model for transcriptional control. *Cell* **169**, 13–23 (2017).
43. W. T. Snead, A. S. Gladfelter, The control centers of biomolecular phase separation: How membrane surfaces, PTMs, and active processes regulate condensation. *Mol. Cell* **76**, 295–305 (2019).
44. W. B. Rogers, W. M. Shih, V. N. Manoharan, Using DNA to program the self-assembly of colloidal nanoparticles and microparticles. *Nat. Rev. Mater.* **1**, 1–14 (2016).
45. L. Cademartiri, K. J. M. Bishop, Programmable self-assembly. *Nat. Mater.* **14**, 2–9 (2015).
46. Y. Zhang *et al.*, Sequential self-assembly of DNA functionalized droplets. *Nat. Commun.* **8**, 21 (2017).
47. R. Niu *et al.*, Magnetic handshake materials as a scale-invariant platform for programmed self-assembly. *Proc. Natl. Acad. Sci. U.S.A.* **116**, 24402–24407 (2019).
48. W. M. Jacobs, Self-assembly of biomolecular condensates with shared components. *arXiv* [Preprint] (2021). https://arxiv.org/abs/2102.12547 (Accessed 4 March 2021).